On-Surface Synthesis and Determination of the Open-Shell Singlet Ground State of Tridecacene

Rafal Zuzak,[†,@] Manish Kumar,[‡,@] Otilia Stoica,[¶,§,@] Diego Soler-Polo,[‡] Jiri Brabec,[‖] Katarzyna Pernal,[⊥] Libor Veis,[‖] Rémi Blieck,[¶] Antonio M. Echavarren,[*,¶,§] Pavel Jelinek,[*,‡,#] and Szymon Godlewski[*,†]

†*Centre for Nanometer-Scale Science and Advanced Materials, NANOSAM, Faculty of Physics, Astronomy and Applied Computer Science, Jagiellonian University, Łojasiewicza 11, PL 30-348 Krakow, Poland*

‡*Institute of Physics, Academy of Sciences of the Czech Republic, Cukrovarnická 10, 162 00, Prague, Czech Republic*

¶*Institute of Chemical Research of Catalonia (ICIQ), Barcelona Institute of Science and Technology, 43007 Tarragona, Spain*

§*Departament de Química Orgànica i Analítica, Universitat Rovira i Virgili, 43007 Tarragona, Spain*

‖*Department of Theoretical Chemistry, J. Heyrovsky Institute of Physical Chemistry, Czech Academy of Sciences, Prague 18200, Czech Republic*

⊥*Institute of Physics, Lodz University of Technology, ul. Wolczanska 219, 90-924 Lodz, Poland*

#*Regional Centre of Advanced Technologies and Materials, Czech Advanced Technology and Research Institute (CATRIN), Palacký University Olomouc, 779 00 Olomouc, Czech Republic*

@*These authors contributed equally*

E-mail: aechavarren@iciq.es; jelinekp@fzu.cz; szymon.godlewski@uj.edu.pl

June 28, 2023

Abstract

The character of the electronic structure of acenes has been the subject of the long-standing discussion. However, convincing experimental evidence of their open-shell character has so far been missing. Here, we present on-surface synthesis of tridecacene molecule by thermal annealing of octahydrotridecacene on Au(111) surface. We characterized the electronic structure of the tridecacene by scanning probe microscopy, which reveals presence of the inelastic signal at 126 meV. We attribute the inelastic signal to the spin excitation from the singlet biradical ground state to triplet excited state. To rationalize the experimental findings we carried out many-body ab-initio calculations as well as model Hamiltonian to take into account the effect of metallic substrate. Moreover, we provide a detailed analysis how the dynamical electron correlation and virtual charge fluctuation between molecule and metallic surface reduces the singlet-triplet band gap. Therefore, this work provides first experimental confirmation of the magnetic character of tridecacene.

Acenes form a family of polycyclic aromatic hydrocarbons composed of linearly fused benzene rings. They have attracted researchers attention in recent decades as archetypical organic semiconductors[1] with potential applications in molecular electronics,[2–4] spintronics[5] or plasmonics[6] due to their high carrier mobility, tunable band gap and reorganization energies as well as expected emergence of ground state magnetic propertie.[7–9] However, the rapidly growing reactivity and instability of acenes with increasing number of annulated rings, which could be rationalized based on Clar's aromatic sextet rule,[10] makes synthesis and characterization of higher acenes very challenging. Therefore despite the recently renewed interest resulting in the synthesis of a series of higher acenes,[11] the theoretically predicted emergence of an open-shell ground state electron configuration has not yet been experimentally doubtlessly demonstrated. To circumvent the described instability higher acenes up to undecacene have been synthesized with the application of cryogenic matrices.[12–15] An alternative, yet attractive approach is based on the on-surface synthesis strategy, in which the

air stable molecular precursors are transformed into parent acenes directly on a substrate surface in ultra-high vaccum conditions enabling generation and characterization of intrinsically unstable molecules. Up to day a range of acenes starting from tetracene up to dodecacene[16–28] have been synthesized on metals based on the surface assisted synthesis approach and the scanning tunneling microscopy/spectroscopy (STM/STS) and non-contact atomic force microscopy (nc-AFM) allowed for their detailed experimental characterization. Some other examples of higher acene synthesis include hexacene,[29,30] heptacene[31] and nonacene[32] synthesized in solid state and recently reported poliacenes mediated by a metal organic framework.[33]

Here, we present the thermally driven on-surface synthesis of tridecacenes on Au(111) and their in-depth characterization by STS measurements corroborated by ab-initio many-body calculations. Our approach is based on the application of air-stable hydrogen protected tridecacene precursors, which are transformed thermally into the longest up to date reported parent acenes on Au(111). The STS measurements and spatial orbital mapping combined with theoretical modelling indicate on the open-shell ground state. This is further supported by the observation of spin excitation initiated by inelastic tunneling electrons, which has not been reported so far for acenes. The STS measurements provide the estimation of the singlet-triplet gap of approximately 126 meV. The experimental findings are rationalized by many-body calculations of the tridecacene, which confirm the open-shell biradical character as well as presence of the singlet-triplet band gap. Moreover, we show that the magnitude of the singlet triplet band gap is affected by the proximity of surface as well as dynamical electron correlation.

RESULTS AND DISCUSSION

On-Surface Synthesis of Tridecacene. Our approach is based on the extension of the previously reported pathway utilizing the so-called hydrogen protected acenes[34] and successfully applied for the on-surface synthesis of the family of higher acenes, from heptacene to undecacene.[20,21] In order to generate the tridecacene on Au(111) we have utilized oc-

tahydrotridecacene **2** (Figure 1) containing eight methylene bridges dividing the aromatic platform and making the starting material air stable. The synthesis of **2** was carried out by a variation of our original synthesis of hydroacenes and related compounds[20,21,35,36] starting by the Sonogashira coupling of previously reported 1,7-enyne $\mathbf{3a}_1$ with new **3b** to provide **4a**, which was desilylated to give **4b** (Figure 1a). Sonogashira coupling of **4b** with 1,4-diiodobenzene gave **5**, which was again coupled with **4b** to give tetra-1,7-enyne **6**. A final four-fold gold(I)-catalyzed [4+2] cycloaddition of **6** gave rise to **2**.

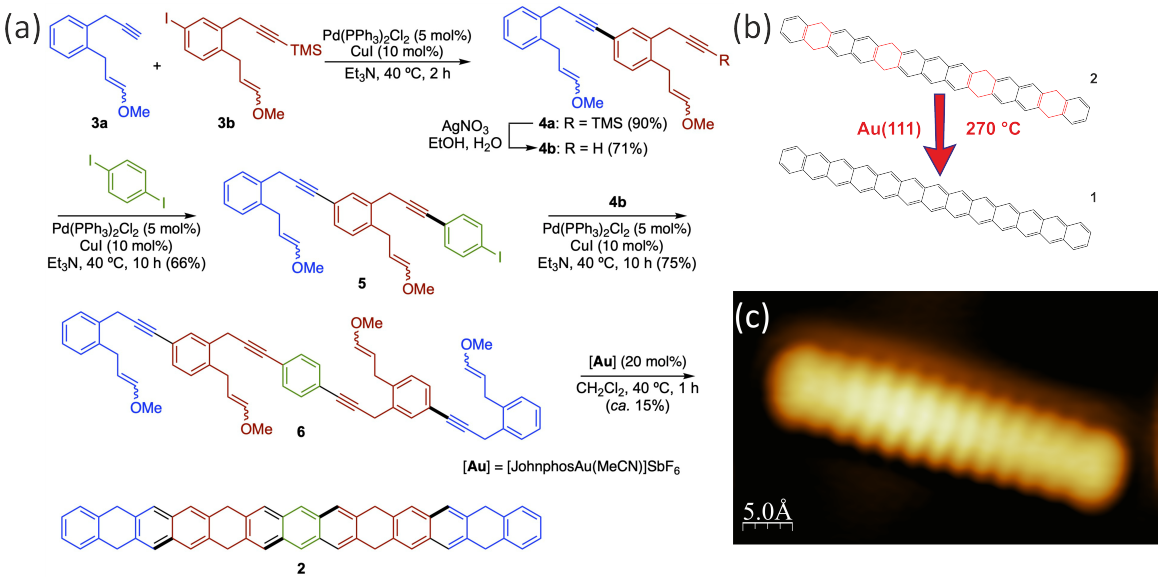

Figure 1: (a) Synthetic path for tridecacene precursor 2,(b) on-surface synthesis scheme leading from **2** to parent tridecacene **1**, (c) high-resolution filled-state STM image of tridecacene thermally synthesized on Au(111), tunneling current: 100 pA, bias voltage: -0.35 V.

The precursors **2** occurred to be not resistant to thermal deposition from powder and therefore we have applied an alternative approach called the dry contact transfer.[37] After deposition on the Au(111) surface the precursors were annealed at 270 $°C$ for 15 minutes. As a result tridecacenes have been generated through thermally driven dehydrogenation as documented by the high resolution filled state STM image shown in Figure 1c, which exhibits presence of expected for parent tridecacene thirteen lobes along the molecule. Similarly as in our previous studies of undecacenes[20] we have encountered the presence of different

isomers within the precursors, which could be visualized within larger scale images by the presence of kinked acenes (see Supplementary Material Figure S15). However, isolated parent tridecacenes **1** could be easily discerned and further they have focused our attention.

Orbital Imaging and spin Excitation. Subsequently we have carried out the single point and spatial dI/dV measurements to probe the local electronic structure of on-surface generated parent tridecacene **1**. The single point dI/dV spectra acquired over the molecule show presence of three distinct and prominent lobes recorded at approximately -0.55 V, -0.35 V and +1.05 V, respectively (Figure 2a). The distribution of the electronic clouds related to these STS peaks is revealed by dI/dV spatial mapping visualized in Figure 2b and corroborated by the calculated dI/dV images based on the Dyson orbitals approach, which will be explained in details in the next paragraph. A closer look into the experimental and calculated dI/dV images reveals good agreement. For instance we can notice two rows of twelve bright lobes in the dI/dV image acquired at -0.55 V, whereas for the dI/dV image recorded at -0.35 V there are two rows, each composed of thirteen lobes along the molecule. At both terminis the two neighboring features are interconnected forming a banana-like shape. Further, in the central part of the molecule the side lobes of the dI/dV image are also becoming combined creating a ladder - like structure. This is in contrast to the images assigned as originating from HOMO (highest occupied molecular orbital) of the closed-shell shorter acenes.[21] Both the experimental and the theoretical empty state dI/dV image is shaped like a eleven-step ladder with two additional features at the ends confirming reasonable compliance between calculations and measurements.

Notably, the single point STS measurements recorded for a narrower voltage range, displayed in Figure 2c, clearly indicates the presence of the symmetric step-like dI/dV curve shape centered around Fermi level. We attribute this feature to the spin-flip inelastic excitation from the ground into the excited state initiated by tunneling electrons. The numerical differentiation of the step-like dI/dV curve yielding the d^2I/dV^2 data visualized in Figure 2c shows the presence of prominent peaks centered at approximately +/- 126 mV. We as-

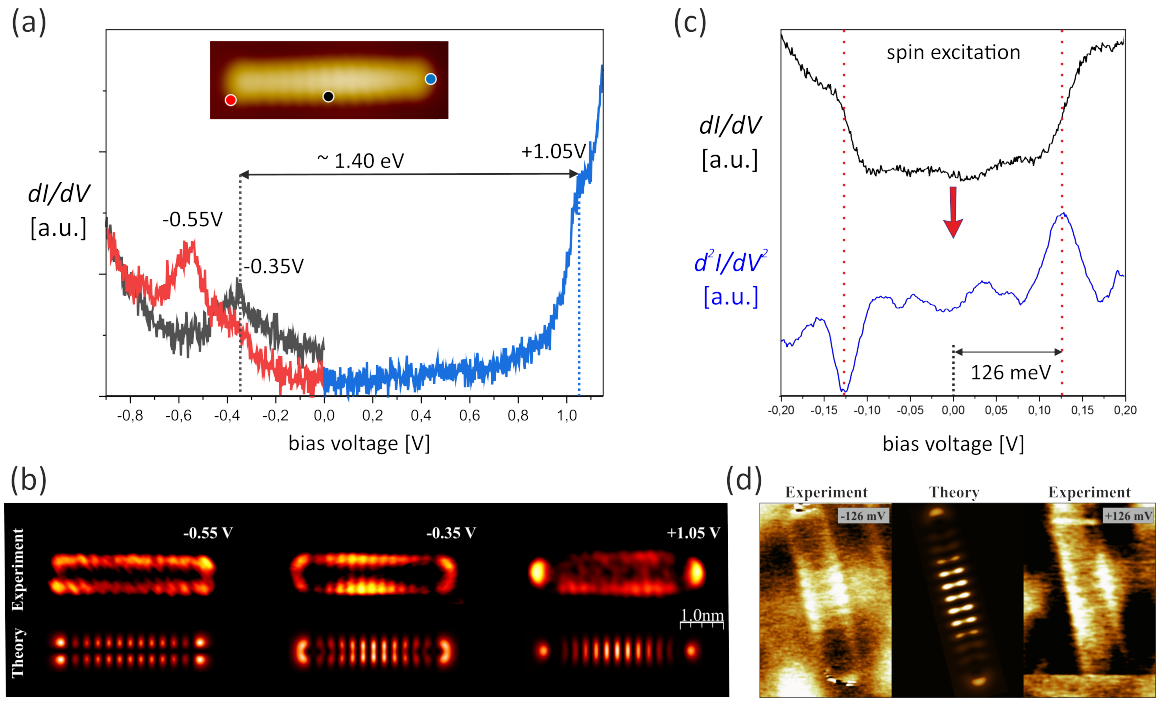

Figure 2: (a) single point STS spectra obtained for tridecacene on Au(111), coloured dots in the inset indicate the lateral tip position during acquisition of the spectra,(b) experimental (top) and calculated (bottom) dI/dV images of tridecacene, (c) single point STS spectra acquired over tridecacene and exhibiting a symmetric step-like appearance (top) together with numerically differentiated d^2I/dV^2 spectra showing presence of pronouneced resonances centred at approximately +/-126 meV, (d) experimental (left, right) and calculated (center) dI/dV spin excitation images for tridecacene, tunneling current: 75 pA

cribe the observed resonances to the transition from the singlet ground state into the triplet excited state of tridecacene, which can be treated as the demonstration of the open-shell character of tridecacene on Au(111). The assignment of the recorded inelastic process to the spin-flip excitation is further supported by the comparison of the experimental dI/dV image with the simulation based on the natural transition orbitals (NTOs), which will be discussed below in the following paragraph. Closer look into the calculated spin excitation image shows presence of the ladder features covering the central part of the molecule, with clearly distinguishable five oblong lobes and supplemented with additional features becoming less pronounced with increasing distance from the molecule center. These lobes are clearly show stronger contrast at the edges and easily discernible blackout in the middle part as visualized in the mid part of Figure 2d. One can note appearance of bright lobes at both ends of tridecacene. Above described features are well reproduced in the experimental dI/dV image acquired for electrons tunneling from the substrate into the tip and presented in the left panel of Figure 2d. The spatial distribution of inelastic excitation recorded for positive voltages, *i.e.* tunneling from the tip into the substrate, also shows the features, however, due to the higher noise level and increased molecule instability they are less pronounced.

Theoretical Analysis of Electronic Structure. To rationalize the open-shell structure and spin excitation of tridecacene, we have employed a variety of theoretical methods, including the exact diagonalization of model Hamiltonians, single reference density functional theory (DFT), and multireference complete active space (CAS)-based approaches, namely the complete active space configuration interaction (CASCI) and the density matrix renormalization group (DMRG)[38,39] coupled with the self-consistent orbital relaxation.[40] CASCCI computations employed the DFT orbitals and were performed in a subspace of the π-orbital space and further corrected for the out-of-CAS dynamical electron correlation by the second-order n-electron valence state perturbation theory (NEVPT2),[41] whereas DMRG computations were performed in the full π-orbital space and corrected by means of the linearized adiabatic connection method (AC0),[42,43] which is the state-of-the-art approach of a

second-order perturbation theory quality suitable for large CAS calculations.

The reason to use the multireference methods mentioned above is the well-known shortcomings of DFT for description of biradicals. In case of the acene family, DFT fails significantly in the estimation of the singlet-triplet energy E_{S-T} (see Figure 3) and overestimates the open-shell character, as discussed later.

Radical Character and Singlet-Triplet Gap in the Gas-Phase. To define the radical character, we have employed the method proposed by Yamaguchi et al.,[44] which for each pair of natural orbitals $HONO-i, LUNO+i$ defines diradical coefficients:

$$Y_d^i = 1 - \frac{2T_i}{(1+T_i^2)},$$

where T_i is given by $T_i = (n_{HONO-i} - n_{LUNO+i})/2$ and n_{HONO-i} and n_{LUNO+i} are the occupation numbers of the HONO and LUNO respectively. According to this criterion, the biradical character is fully developed for values Y_d^0 higher than 0.5. These natural orbitals are obtained by diagonalizing the 1-particle reduced density matrix.[45] Deviations from the ideal occupancies of 0 (indicating an empty orbital) or 2 (representing a fully occupied orbital) indicate an increasing radical character within the system, as picked up by Yamaguchi's coefficients Y_d^i defined above. We have calculated $Y_d^0 + Y_d^1$ at different levels of theory (see Figure 3a) to ascribe a radical character to acenes of different length. Using this criterion, DFT calculations predict the full biradical character for nonacene and, furthermore, from the heptacene on, the open shell structures (relaxed structures from spin polarized calculations) are lower in energy than the closed shell ones (relaxed structures from spin unpolarized calculations).

On the other hand, we have also calculated the singlet-triplet excitation energy, which for the case of tridecacene should be compared to experimentally measured spin excitation. DFT revealed an erroneous non-monotonous trend in the singlet-triplet energy gap (E_{S-T})

of acenes (see Figure 3a).

Due to the shortcomings of DFT, reflected in the wrong description of the singlet-triplet energy gap and the overestimation of the radical character, we employed multireference CASCI[46] calculations with an active space consisting of up to 12 electrons in 12 π orbitals, which can properly describe the radical character of acenes. To ensure the reliability of our findings, we benchmarked these CASCI results against full π active space DMRG calculations, as shown in Figure 3a.

The comparison between CASCI and DMRG calculations shows that we have well-converged results in the π-subspace and predict an open-shell structure for the undecacene and larger acenes, which present a clear diradical character, see Figure 3b. However, we have not detected the spin excitation in STS measurements for undecacene. It was also not reported for dodecacene,[22] suggesting that the open-shell character was not fully developed yet. The tridecacene is the first acene in the series with an open-shell configuration corroborated by experimentally detected spin excitation. However, the theoretically predicted spin excitation is 300 meV according to both CASCI and DMRG calculations, which is still far from the experimental value of 126 meV.

Two scenarios that could potentially explain these discrepancies are 1) the effect of the dynamical electron correlation involving electron-hole excitation beyond π-electron active spaces and 2) the effect of the proximity of a metallic substrate. Next, we will discuss the effect of both factors on the radical character of acenes as well as on the singlet-triplet band gap.

Effect of the Dynamical Electron Correlation. One of the most common options to account for out-of-CAS dynamical electron correlation consists of usage of many-body perturbation theory.[41,47] The idea is that starting from the exact many-body CAS wavefunction, we can perturbatively involve the effect of all the orbitals, including the deep σ orbitals of the molecules.

The NEVPT2 method, commonly used for electronic structure calculations, primarily

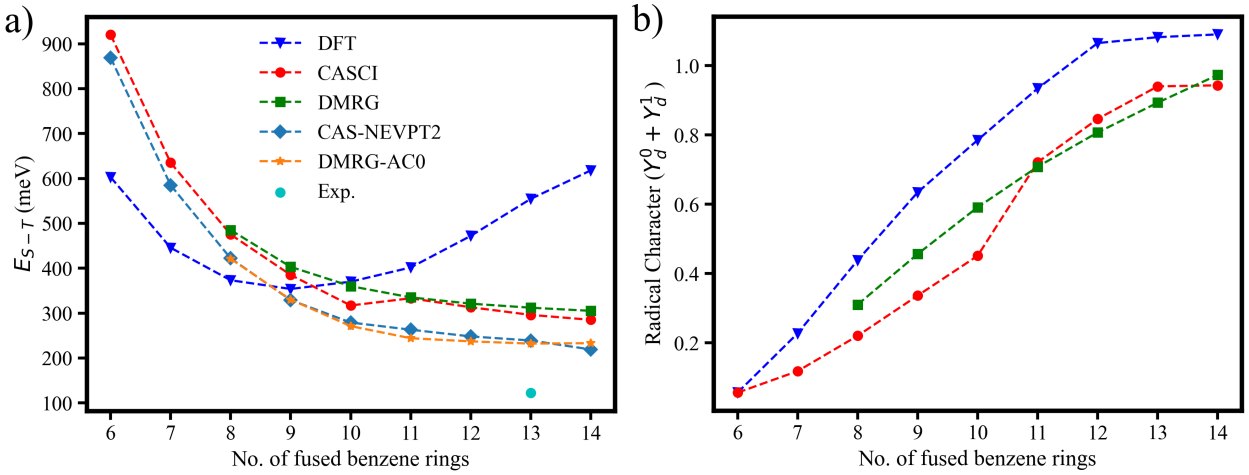

Figure 3: a) Comparison of Singlet-Triplet energy gap with DFT/PBE0, CASCI(12,12), CAS-NEVPT2, DMRG(full π space), DMRG-AC0 in meV, see also Table S1. b) Comparison of diradical character with DFT/PBE0, CASCI(12,12), and DMRG(full π space), see also Table S2.

focuses on correcting energy values. In case of small active space CASCI computations, we have carried out the NEVPT2 energy corrections, the full π-orbital DMRG calculations were corrected by means of AC0. The reason for the later is that the size of CAS of studied molecules is far beyond the limits of the conventional NEVPT2 (notice that for tetradecacene, CAS comprises 58 π orbitals). In the context of the Singlet-Triplet gap, NEVPT2 and AC0 provide very similar energy gaps and demonstrate a minor yet discernible influence, see Figure 3a.

This observation prompts further investigation into the impact of the σ orbitals on the electronic structure, specifically examining the occupancies of natural orbitals. While previous studies have shown satisfactory convergence of results concerning the π orbitals (detailed tables can be found in the supplementary information), we adopt a reduced set of π orbitals and explicitly explore the effects of the σ orbitals. To accomplish this, we determine the exact wavefunction using the CASCI method within this reduced active space.

Table S3 shows the effect of including up to three σ orbitals in an active space of six π orbitals and then solving the resulting ab initio Hamiltonian by exact diagonalization in an active space of 12 electrons CAS(12,9), meaning there are six π orbitals contributing with

six electrons, and three σ orbitals contributing 6 electrons. This simple model shows how the explicit inclusion of just a few σ orbitals can affect the spin excitation, and its interest will be further explained below in connection with the effect of the substrate.

Effect of the Surface in the Singlet-Triplet Energy Gap. It is generally known that the electronic structure of molecules physically adsorbed on metal surfaces is partially modified by the reduction of the HOMO-LUMO band gap.[48] Thus, to account for the metallic substrate, we have chosen as a first approximation the application of a scissor operator to reduce the molecular band gap. The scissor operator is applied on the single electron part of the molecular Hamiltonian, which is used for the many-body CASCI calculations. As shown in Table S4, such contribution has a very minor effect and does not change the overall qualitative picture of the singlet-triplet energy E_{S-T}.

Therefore, we consider a more sophisticated model to account for the metallic substrate within a many-body picture. We couple the molecular levels to an effective chain made consisting of seven coupled sites that mimic the effect of the substrate, see Figure 4a:

$$\hat{H} = \hat{H}_{\text{CAS}} + \hat{H}_{\text{chain}} + \hat{H}_{\text{int}}.$$

Here $\hat{H}_{\text{CAS}}$ is the *ab initio* CASCI Hamiltonian; $\hat{H}_{\text{chain}}$ is a one-electron Hamiltonian describing the chain,

$$\hat{H}_{\text{chain}} = -T \sum_{m=1,\sigma}^{N-1} \hat{d}^{\dagger}_{m+1\sigma} \hat{d}_{m\sigma} + \text{h.c.} + \varepsilon_F \sum_{m=1,\sigma}^{N} \hat{d}^{\dagger}_{m\sigma} \hat{d}_{m\sigma},$$

$$\hat{H}_{\text{int}} = -\sum_{j\sigma} t_j \hat{d}^{\dagger}_{1\sigma} \hat{C}_{j\sigma} + \text{h.c},$$

where the $\hat{C}_{j\sigma}$ are the anihilation operators of the molecular orbitals of the active space, with t_j a hopping that is largest, τ, for the HOMO/LUMO orbitals and decays with energy, $t_j = \tau \exp\left(-|\varepsilon_j - \varepsilon_F|\right)$ (with ε_j the effective energy of the j-th level, ε_F the Fermi energy and ε_H the effective energy of the HOMO orbital). We have explored the effect of this model for different values of T and ε_F as well as for t ranging between 0 and 0.5 eV, where the

charge and spin of the molecule are still good quantum numbers (see Figure S16)

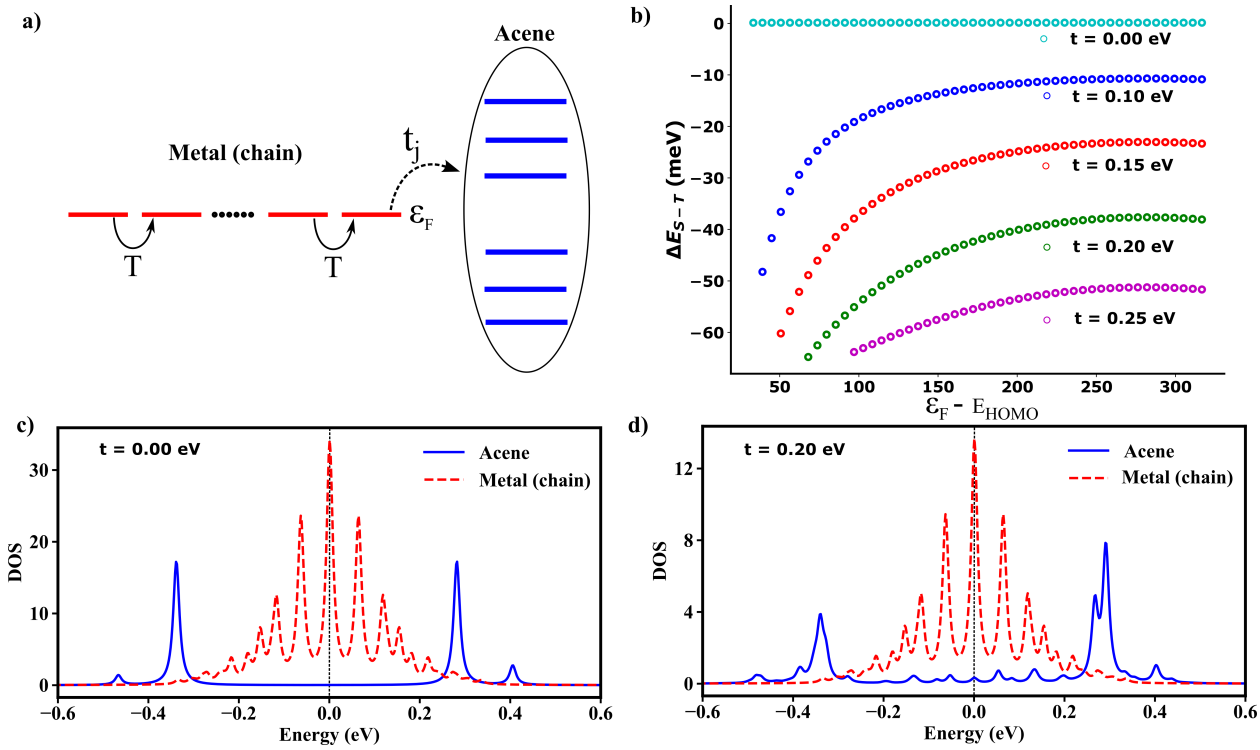

Figure 4: a) Schematic representation of the model Hamiltonian including metallic substrate. b) Renormalization in Singlet-Triplet energy gap due to coupling between metal-chain and acene molecular orbitals for different values of t. c) Density of states (DOS) projected over acene molecular orbitals and metal chain when they are not coupled with each other and dashed line shows the metal chain Fermi (ε_F) level. d) Density of states (DOS) projected over acene molecular orbitals and metal chain when the coupling between them is 0.2 eV, and dashed line shows the metal chain fermi (ε_F) level.

Figure 4b displays evolution of the singlet-triplet energy E_{S-T} as function of the coupling t as well as energy diferece between Fermi level of metallic substrate and HOMO level. Here we explore a limit of small coupling $t \approx 0 - 0.25$eV where there are only slight changes in the DOS compared to the free-standing molecule, see Figures 4c,d. This situation mimics the physisorption regime of tridecacene on metallic substrate. In general, we observe that an increasing coupling t decreases the singlet-triplet gap. Even with a relatively small coupling strength of τ =0.2 eV, there is an approximate renormalization of 60 meV in the singlet-triplet energy gap. This renormalization is caused by the emergence of new in-gap interface electronic states located between the HOMO and the LUMO, see Figures 4d. The presence of

these in-gap states facilitate virtual charge fluctuation between molecule and surface causing an effective screening of exchange coupling in the molecule. Consequently, this reduces the singlet-triplet energy E_{S-T}.

Second, as shown in Figure 4b the proximity of HOMO orbital to the Fermi level of metallic surface also promotes virtual charge fluctuation between molecule and surface. Consequently the presence of charge fluctuation decreases the singlet-triplet energy E_{S-T}. We should stress that we explore only the regime of a very weak mixed valence regime, where the molecular spin is still good quantum number and molecule retains practically its own charge, see Figure S16.

To summarize, we see that the presence of a metallic surface, even if only in the physisorbed regime, leads to the presence of non-negligible charge fluctuation between the molecule and the surface, which results in a decrease in the singlet-triplet energy E_{S-T}. When the molecule-substrate interaction is strengthened or the HOMO orbital is located close to the Fermi level, the effect of charge fluctuation increases and can lead to a situation where the spin of the molecule is no longer a well-defined quantum number. One of the consequences of this mixed valence regime will be the impossibility of detecting spin excitation. This may be one of the reasons why the spin excitation signal was not observed for shorter acenes featuring the biradical character.

Combining Dynamic Correlation and Substrate Effects. Finally, we combine together two effects discussed previously, i.e. dynamical electron correlation including excitations from σ orbitals and the proximity of metallic substrate. Namely, we would like to demonstrate the additive nature of both corrections on the singlet-triplet gap. In order to make the CASCI calculations tractable, we had to reduce active space of the molecule. Thus, in our model we consider an active space of four π orbitals and three σ orbitals of the acene, while the metallic surface is represented by a chain made of four sites, which couple to the π orbitals. As above, the many-body Hamiltonian of the $\pi + \sigma$ system is defined *ab initio* from the molecular Hamiltonian and the DFT orbitals, whereas the chain of four

levels is described by a tight-binding Hamiltonian, with one level from the chain coupled to the π orbitals through hopping t. This calculation shows that the correction to the singlet-triplet gap from the σ orbitals, Δ_σ and the correction from the model for the substrate, Δ_s combine to yield a correction $\simeq \Delta_\sigma + \Delta_s$ when we simultaneously include σ orbitals and the metallic chain. As seen above, the correction provided by the chain simulating the substrate is about $\sim$ -50 meV, and the correction for the dynamical correlation from NEVPT2 or AC0 is similarly -60 meV for the tridecacene, which yields an overall correction of ~ -110 meV to be added to the estimated singlet-triple gap in π space.

Dyson Orbitals and Spin Excitation Map. To rationalize dI/dV maps acquired for molecules featuring strongly multireference character, one should, in principle, go beyond single determinant molecular orbital picture offered by DFT calculations. Therefore, we employed the concept of the Dyson orbitals[49] to simulated dI/dV maps shown in Figure 2b. The Dyson orbitals represent processes of removal and addition of one electron respectively, during the tunneling process. In the case of dI/dV maps mapping empty molecular states, we used CASCI(13,12) and CASCI(12,12) calculations to obtain Dyson orbital φ_{LUMO} corresponding to transition between the ground state wave function for neutral (Ψ_0) and charge N+1 ($\Psi_{+,0}$):

$$\varphi_{\mathrm{LUMO}}(x) = \sqrt{N+1} \int \Psi_0(x_1, \cdots, x_{12}) \Psi_{+,0}(x, x_1, \cdots, x_{12}) dx_1 \cdots dx_{12}.$$

Similarly, we calculated Dyson orbitals corresponding for a single electron withdrawal from occupied molecular orbitals:

$$\varphi_{\mathrm{HOMO}}(x) = \sqrt{N} \int \Psi_0(x, x_1, \cdots, x_{11}) \Psi_{-,0}(x_1, \cdots, x_{11}) dx_1 \cdots dx_{11},$$

$$\varphi_{\mathrm{HOMO\text{-}1}}(x) = \sqrt{N} \int \Psi_0(x, x_1, \cdots, x_{11}) \Psi_{-,1}(x_1, \cdots, x_{11}) dx_1 \cdots dx_{11},$$

where $\Psi_{-,0}$ and $\Psi_{-,1}$ are respectively the ground state and first excited state of the system

with one less electron N-1 (at the level of CAS(11,12)). These three orbitals correspond to the three peaks in Figure 2 (a).

On the other hand, to assess the spatial variation of dI/dV maps corresponding to the spin excitation signal (see Figure 2d), we have calculated the so-called Natural Transition Orbitals (NTO)[50] for the spin-flip operator mimicking transition from the singlet to the triplet ground state. NTO orbitals are obtained from the diagonalization of the matrix $TT^{\dagger}$, where the matrix T is given by elements

$$T_{jk} = \langle \Psi_{\text{triplet}} | \hat{C}^{\dagger}_{j\uparrow} \hat{C}_{k\downarrow} | \Psi_{\text{singlet}} \rangle,$$

where the indices j, k run over the active orbitals. We have constructed such matrices from CASCI(12,12) calculations, and the corresponding orbitals are shown in Figure 5, whereas their dI/dV maps are shown in Figure 2.

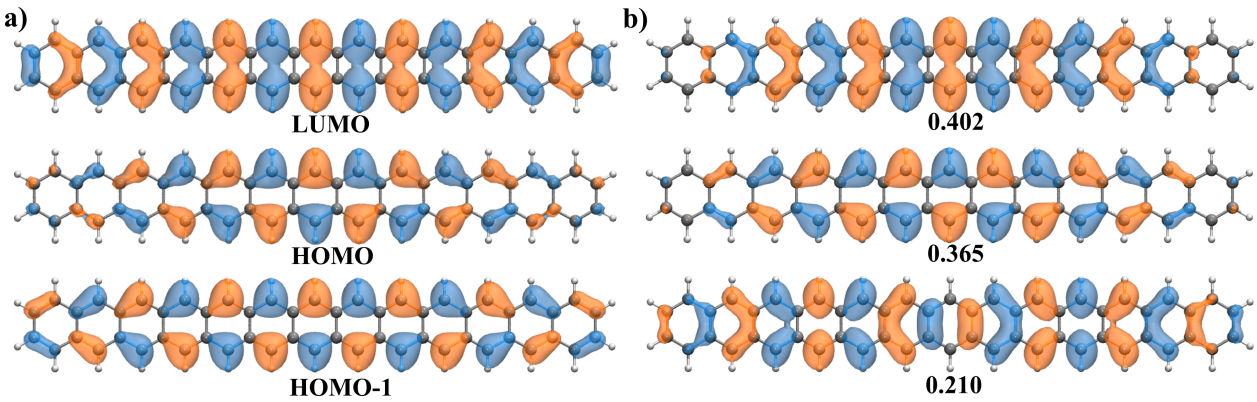

Figure 5: a) Dyson orbitals for LUMO, HOMO, and HOMO-1 b) Natural Transition Orbitals corresponding to three dominant channels with their respective eigenvalue mentioned at the bottom.

CONCLUSIONS

This study showed the potential of on-surface chemistry to synthesize new organic compounds that are not available by traditional organic synthesis methods. Namely, we presented the on-surface synthesis of tridecacene on Au(111) surface, which provided the longest acene synthesized up to now. Moreover, the good match between scanning tunnelling spectroscopy

and the state-of-the-art many-body calculations confirmed the open-shell biradical character of tridecacene. Thus, this work provided unequivocal proof of the open-shell nature of long acences. Furthermore, we performed a detailed theoretical analysis of the influence of the dynamical electron correlation and the presence of a metal surface on the singlet-triplet gap. We found that both effects combine synergically and result in approx. 110 meV reduction of the singlet-triplet gap with respect to the case of a free-standing molecule.

METHODS

Experiment. The STM/STS (Scienta Omicron GmbH) experiment was carried out in ultra-high vacuum conditions (UHV, base pressure $10^{-10} mbar$), in liquid helium temperature (4.5 K). The moncrystalline Au (111) sample was prepared by cyclical annealing and bombardment by Ar+ ions. The precursor molecules were deposited on an atomically clean Au (111) surface using the DCT (dry contact transfer) method.[37] Fiberglass, properly cleaned, was used as a filament. After precursors application on the surface, the sample was annealed at approximately 270 $^{\circ}C$ for 15 minutes. As STM/STS probes etched Pt-Ir tips were used. The dI/dV measurements were collected using the lock-in technique (f = 680Hz, Amp. = 10-15 mV). Before the dI/dV data acquisition the tip was stabilized with the starting voltage of the selected STS spectra. **Calculations.** We optimized the structures of free-standing acenes from 2 to 14-annulated benzene rings using the local orbital DFT code FHI-AIMS[51] with the PBE0 functional.[52] The DFT energy calculations of the singlet and triplet states with the PBE0 functional and def2-SVP basis, as well as the strongly contracted NEVPT2 calculations were carried out in the ORCA package.[53] CASCI calculations with the DFT orbitals were performed in our in-house exact diagonalization code. From the eigenvectors we constructed Dyson orbitals and NTO orbitals as detailed in the text. To generate the dI/dV maps of Fig. 2 from these orbitals we employed the Proble Particle code[54] with a simulated s-like tip.

All DMRG calculations presented above corresponded to the orbital optimized DMRG, i.e. DMRG-SCF.[40] These calculations were carried out in ORCA[53] interfaced to the MOL-

MPS DMRG code[55] and employed the cc-pVDZ basis set, split-localized RHF orbitals as an initial guess, and fixed DMRG bond dimensions $M = 1000$. The one- and two-electron reduced density matrices needed for the AC0 method were obtained from the more accurate DMRG calculations on top of the optimized DMRG-SCF orbitals, which employed the dynamical block state selection[56] and the predefined truncation error of 10^{-6}. The AC0 calculations were performed in GammCor.[57]

Author contributions

S.G., A.M.E. and P.J. conceived the project. O.S. and R.B. carried out the tridecacene precursor synthesis under the supervision of A.M.E. R.Z.conducted the on-surface synthesis and low-temperature STM/STS measurements with support from S.G. M.K., D.S., L.V., K.P., J.B. and P.J. carried out theoretical calculations. S.G. and P.J. prepared the manuscript with feedback from all other authors. All authors have given approval to the final version of the manuscript.

Funding

We acknowledge financial support from the National Science Center, Poland (2017/26/E/ST3/-00855), MCIN/AEI/10.13039/501100011033 (PID2019-104815GB-I00 and CEX2019-000925-S), the AGAUR (2021 SGR 01256), and CERCA Program/Generalitat de Catalunya. We acknowledge support from the CzechNanoLab Research Infrastructure supported by MEYS CR (LM2023051) and the GACR project no. 23-05486S. This work was also supported by the Czech Ministry of Education, Youth and Sports from the Large Infrastructures for Research, Experimental Development and Innovations project "IT4Innovations National Supercomputing Center-LM2015070 and the Center for Scalable and Predictive methods for Excitation and Correlated phenomena (SPEC), which is funded by the U.S. Department of Energy (DOE), Office of Science, Office of Basic Energy Sciences, the Division of Chemical Sciences, Geosciences, and Biosciences.

Notes

The authors declare no competing financial interest.

References

(1) Anthony, J. E. The Larger Acenes: Versatile Organic Semiconductors. *Angewandte Chemie International Edition* **2008**, *47*, 452–483.

(2) Wang, C.; Dong, H.; Hu, W.; Liu, Y.; Zhu, D. Semiconducting π-Conjugated Systems in Field-Effect Transistors: A Material Odyssey of Organic Electronics. *Chemical Reviews* **2012**, *112*, 2208–2267, PMID: 22111507.

(3) Xiang, D.; Wang, X.; Jia, C.; Lee, T.; Guo, X. Molecular-Scale Electronics: From Concept to Function. *Chemical Reviews* **2016**, *116*, 4318–4440, PMID: 26979510.

(4) Ye, Q.; Chi, C. Recent Highlights and Perspectives on Acene Based Molecules and Materials. *Chemistry of Materials* **2014**, *26*, 4046–4056.

(5) Han, W.; Kawakami, R.; Gmitra, M.; et al., Graphene spintronics. *Nature Nanotech* **2014**, *9*, 794–807.

(6) Guidez, E. B.; Aikens, C. M. Origin and TDDFT Benchmarking of the Plasmon Resonance in Acenes. *The Journal of Physical Chemistry C* **2013**, *117*, 21466–21475.

(7) Bendikov, M.; Duong, H. M.; Starkey, K.; Houk, K. N.; Carter, E. A.; Wudl, F. Oligoacenes: Theoretical Prediction of Open-Shell Singlet Diradical Ground States. *Journal of the American Chemical Society* **2004**, *126*, 7416–7417, PMID: 15198569.

(8) Hachmann, J.; Dorando, J. J.; Avilés, M.; Chan, G. K.-L. The radical character of the acenes: A density matrix renormalization group study. *The Journal of Chemical Physics* **2007**, *127*, 134309.

(9) Yang, Y.; Davidson, E. R.; Yang, W. Nature of ground and electronic excited states of higher acenes. *Proceedings of the National Academy of Sciences* **2016**, *113*, E5098–E5107.

(10) Clar, E. Aromatic sextet. **1972**,

(11) Tönshoff, C.; Bettinger, H. F. Pushing the Limits of Acene Chemistry: The Recent Surge of Large Acenes. *Chemistry – A European Journal* **2021**, *27*, 3193–3212.

(12) Mondal, R.; Adhikari, R. M.; Shah, B. K.; Neckers, D. C. Revisiting the stability of hexacenes. *Organic letters* **2007**, *9 13*, 2505–8.

(13) Mondal, R.; Shah, B. K.; Neckers, D. C. Photogeneration of Heptacene in a Polymer Matrix. *Journal of the American Chemical Society* **2006**, *128*, 9612–9613, PMID: 16866498.

(14) Tönshoff, C.; Bettinger, H. Photogeneration of Octacene and Nonacene. *Angewandte Chemie International Edition* **2010**, *49*, 4125–4128.

(15) Shen, B.; Tatchen, J.; Sanchez-Garcia, E.; Bettinger, H. F. Evolution of the Optical Gap in the Acene Series: Undecacene. *Angewandte Chemie International Edition* **2018**, *57*, 10506–10509.

(16) Pavliček, N.; Mistry, A.; Majzik, Z.; et al., Synthesis and characterization of triangulene. *Nature Nanotech* **2017**, *12*, 308–311.

(17) Krüger, J.; Eisenhut, F.; Alonso, J. M.; Lehmann, T.; Guitián, E.; Pérez, D.; Skidin, D.; Gamaleja, F.; Ryndyk, D. A.; Joachim, C.; Peña, D.; Moresco, F.; Cuniberti, G. Imaging the electronic structure of on-surface generated hexacene. *Chem. Commun.* **2017**, *53*, 1583–1586.

(18) Dinca, L. E.; Fu, C.; Macleod, J. M.; Lipton-Duffin, J.; Brusso, J. L.; Szakacs, C. E.; Ma, D.; Perepichka, D. F.; Rosei, F. Unprecedented transformation of tetrathienoanthracene into pentacene on Ni(111). *ACS nano* **2013**, *7 2*, 1652–7.

(19) Krüger, J.; Eisenhut, F.; Skidin, D.; Lehmann, T. D.; Ryndyk, D. A.; Cuniberti, G.; García, F.; Alonso, J. M.; Guitián, E.; Pérez, D.; Peña, D.; Trinquier, G.; Malrieu, J.;

Moresco, F.; Joachim, C. Electronic Resonances and Gap Stabilization of Higher Acenes on a Gold Surface. *ACS nano* **2018**, *12 8*, 8506–8511.

(20) Zuzak, R.; Dorel, R.; Kolmer, M.; Szymonski, M.; Godlewski, S.; Echavarren, A. M. Higher Acenes by On-Surface Dehydrogenation: From Heptacene to Undecacene. *Angewandte Chemie International Edition* **2018**, *57*, 10500–10505.

(21) Zuzak, R.; Dorel, R.; Krawiec, M.; Such, B.; Kolmer, M.; Szymonski, M.; Echavarren, A. M.; Godlewski, S. Nonacene Generated by On-Surface Dehydrogenation. *ACS Nano* **2017**, *11*, 9321–9329, PMID: 28817255.

(22) Eisenhut, F.; Kühne, T.; García, F.; Fernández, S.; Guitián, E.; Pérez, D.; Trinquier, G.; Cuniberti, G.; Joachim, C.; Peña, D.; Moresco, F. Dodecacene Generated on Surface: Reopening of the Energy Gap. *ACS Nano* **2020**, *14*, 1011–1017, PMID: 31829618.

(23) Urgel, J.; Mishra, S.; Hayashi, H.; et al., On-surface light-induced generation of higher acenes and elucidation of their open-shell character. *Nat Commun* **2019**, *10*.

(24) Krüger, J.; García, F.; Eisenhut, F.; Skidin, D.; Alonso, J. M.; Guitián, E.; Pérez, D.; Cuniberti, G.; Moresco, F.; Peña, D. Decacene: On-Surface Generation. *Angewandte Chemie* **2017**, *56 39*, 11945–11948.

(25) Zugermeier, M.; Gruber, M.; Schmid, M.; Klein, B. P.; Ruppenthal, L.; Müller, P.; Einholz, R.; Hieringer, W.; Berndt, R.; Bettinger, H. F.; Gottfried, J. M. On-surface synthesis of heptacene and its interaction with a metal surface. *Nanoscale* **2017**, *9*, 12461–12469.

(26) Eimre, K.; Urgel, J.; Hayashi, H.; et al., On-surface synthesis and characterization of nitrogen-substituted undecacenes. *Nat Commun* **2022**, *13*.

(27) Lohr, T. G.; Urgel, J. I.; Eimre, K.; Liu, J.; Di Giovannantonio, M.; Mishra, S.; Berger, R.; Ruffieux, P.; Pignedoli, C. A.; Fasel, R.; Feng, X. On-Surface Synthesis

of Non-Benzenoid Nanographenes by Oxidative Ring-Closure and Ring-Rearrangement Reactions. *Journal of the American Chemical Society* **2020**, *142*, 13565–13572, PMID: 32657120.

(28) Colazzo, L.; Mohammed, M. S. G.; Dorel, R.; Nita, P.; García Fernández, C.; Abufager, P.; Lorente, N.; Echavarren, A. M.; de Oteyza, D. G. On-surface synthesis of heptacene on Ag(001) from brominated and non-brominated tetrahydroheptacene precursors. *Chem. Commun.* **2018**, *54*, 10260–10263.

(29) Watanabe, M.; Chang, Y.; Liu, S.; Chao, T.; Goto, K.; Islam, M.; Yuan, C.; Tao, Y.; Shinmyozu, T.; Chow, T. The synthesis, crystal structure and charge-transport properties of hexacene. *Nature Chemistry* **2012**, *4*, 574–578.

(30) Monahan, N.; Sun, D.; Tamura, H.; et al., Dynamics of the triplet-pair state reveals the likely coexistence of coherent and incoherent singlet fission in crystalline hexacene. *Nature Chemistry* **2017**, *9*, 341–346.

(31) Einholz, R.; Fang, T.; Berger, R.; Grüninger, P.; Früh, A.; Chassé, T.; Fink, R. F.; Bettinger, H. F. Heptacene: Characterization in Solution, in the Solid State, and in Films. *Journal of the American Chemical Society* **2017**, *139*, 4435–4442, PMID: 28319405.

(32) Jančařík, A.; Holec, J.; Nagata, Y.; et al., Preparative-scale synthesis of nonacene. *Nature Chemistry* **2022**, *13*.

(33) Kitao, T.; Miura, T.; Nakayama, R.; et al., Synthesis of polyacene by using a metal–organic framework. *Nat. Synth* **2023**,

(34) Athans, A. J.; Briggs, J. B.; Jia, W.; Miller, G. P. Hydrogen-protected acenes. *J. Mater. Chem.* **2007**, *17*, 2636–2641.

(35) Dorel, R.; McGonigal, P. R.; Echavarren, A. M. Hydroacenes Made Easy by Gold(I) Catalysis. *Angewandte Chemie International Edition* **2016**, *55*, 11120–11123.

(36) Zuzak, R.; Stoica, O.; Blieck, R.; Echavarren, A. M.; Godlewski, S. On-surface synthesis and intermolecular cycloadditions of indacenoditetracenes, antiaromatic analogues of undecacene. *ACS nano* **2020**, *15*, 1548–1554.

(37) Albrecht, P. M.; Lyding, J. W. Ultrahigh-vacuum scanning tunneling microscopy and spectroscopy of single-walled carbon nanotubes on hydrogen-passivated Si(100) surfaces. *Applied Physics Letters* **2003**, *83*, 5029–5031.

(38) White, S. R. Density matrix formulation for quantum renormalization groups. *Phys. Rev. Lett.* **1992**, *69*, 2863.

(39) Chan, G. K.-L.; Sharma, S. The Density Matrix Renormalization Group in Quantum Chemistry. *Annu. Rev. Phys. Chem.* **2011**, *62*, 465–481.

(40) Zgid, D.; Nooijen, M. The density matrix renormalization group self-consistent field method: Orbital optimization with the density matrix renormalization group method in the active space. *J. Chem. Phys.* **2008**, *128*, 144116.

(41) Angeli, C.; Cimiraglia, R.; Evangelisti, S.; Leininger, T.; Malrieu, J.-P. Introduction of n-electron valence states for multireference perturbation theory. *J. Chem. Phys.* **2001**, *114*, 10252–10264.

(42) Pernal, K. Electron Correlation from the Adiabatic Connection for Multireference Wave Functions. *Phys. Rev. Lett.* **2018**, *120*.

(43) Pastorczak, E.; Pernal, K. Correlation Energy from the Adiabatic Connection Formalism for Complete Active Space Wave Functions. *J. Chem. Theory Comput.* **2018**, *14*, 3493–3503.

(44) Yamaguchi, K.; Takahara, Y.; Fueno, T.; Houk, K. Extended Hartree-Fock (EHF) theory of chemical reactions: III. Projected Møller-Plesset (PMP) perturbation wave-

functions for transition structures of organic reactions. *Theoretica chimica acta* **1988**, *73*, 337–364.

(45) Löwdin, P.-O. Quantum Theory of Many-Particle Systems. I. Physical Interpretations by Means of Density Matrices, Natural Spin-Orbitals, and Convergence Problems in the Method of Configurational Interaction. *Phys. Rev.* **1955**, *97*, 1474–1489.

(46) Levine, B. G.; Durden, A. S.; Esch, M. P.; Liang, F.; Shu, Y. CAS without SCF—Why to use CASCI and where to get the orbitals. *Journal of Chemical Physics* **2021**, *154*.

(47) Andersson, K.; Malmqvist, P.-Å.; Roos, B. O. Second-order perturbation theory with a complete active space self-consistent field reference function. *J. Chem. Phys.* **1992**, *96*, 1218–1226.

(48) Neaton, J. B.; Hybertsen, M. S.; Louie, S. G. Renormalization of molecular electronic levels at metal-molecule interfaces. *Physical review letters* **2006**, *97*, 216405.

(49) Ortiz, J. V. Dyson-orbital concepts for description of electrons in molecules. *The Journal of Chemical Physics* **2020**, *153*, 070902.

(50) Martin, R. L. Natural transition orbitals. *The Journal of Chemical Physics* **2003**, *118*, 4775–4777.

(51) Blum, V.; Gehrke, R.; Hanke, F.; Havu, P.; Havu, V.; Ren, X.; Reuter, K.; Scheffler, M. Ab initio molecular simulations with numeric atom-centered orbitals. *Computer Physics Communications* **2009**, *180*, 2175–2196.

(52) Adamo, C.; Barone, V. Toward reliable density functional methods without adjustable parameters: The PBE0 model. *The Journal of chemical physics* **1999**, *110*, 6158–6170.

(53) Neese, F. The ORCA program system. *Wiley Interdisciplinary Reviews: Computational Molecular Science* **2012**, *2*, 73–78.

(54) Hapala, P.; Temirov, R.; Tautz, F. S.; Jelínek, P. Origin of High-Resolution IETS-STM Images of Organic Molecules with Functionalized Tips. *Phys. Rev. Lett.* **2014**, *113*, 226101.

(55) Brabec, J.; Brandejs, J. F.; Kowalski, K.; Xantheas, S. S.; Legeza, O.; Veis, L. Massively parallel quantum chemical density matrix renormalization group method. *Journal of Computational Chemistry* **2020**, *42*, 534 – 544.

(56) Legeza, Ö.; Röder, J.; Hess, B. Controlling the Accuracy of the Density-matrix Renormalization-Group Method: The Dynamical Block State Selection Approach. *Phys. Rev. B* **2003**, *67*, 125114.

(57) Pernal, K.; Hapka, M.; Przybytek, M.; Modrzejewski, M.; Sokół, A. GammCor code. `https://github.com/pernalk/GAMMCOR`, 2022.